A Novel Maximum Power Point Tracker for PV Panels Using Switching Frequency Modulation

K. K. Tse, *Member, IEEE*, M. T. Ho, *Student Member, IEEE*, Henry S.-H. Chung, *Member, IEEE*, and S. Y. (Ron) Hui, *Senior Member, IEEE*

***Abstract*—A novel technique for efficiently extracting maximum power from photovoltaic (PV) panels is presented. The power conversion stage, which is connected between a PV panel and a load or bus, is a SEPIC or Cuk converter or their derived circuits operating in discontinuous inductor–current or capacitor–voltage mode. Method of locating the maximum power point (MPP) is based on injecting a small-signal sinusoidal perturbation into the switching frequency and comparing the ac component and the average value of the panel terminal voltage. Apart from not requiring any sophisticated digital computation of the panel power, the proposed technique does not approximate the panel characteristics and can globally locate the MPP under wide insolation conditions. The tracking capability has been verified experimentally with a 10 W solar panel under a controlled experimental setup. Performances under the steady state and in the large-signal change of the insolation level will be given.**

***Index Terms*—DC–DC power conversion, maximum-power-point tracking, photovoltaic.**

I. Introduction

PHOTOVOLTAIC (PV) technology has developed rapidly over the last two decades from a small scale, specialist industry supplying the United States space program to a broadly based global activity [1]. Solar panel is the fundamental energy conversion component of photovoltaic (PV) systems. Its conversion efficiency depends on many extrinsic factors, such as insolation (incident solar radiation) levels, temperature, and load condition.

There are three major approaches for maximizing power extraction in medium- and large-scale systems. They are sun tracking, maximum power point (MPP) tracking or both. For the small-scale systems, MPP tracking is popular for economical reasons. Various methods including power matching scheme [2], [3], curve-fitting technique [4], [5], perturb-and-observe method [6], [7], and incremental conductance technique [8], [9] have been proposed.

The power-matching scheme requires the selected solar panels to have suitable output characteristics or configurations that can be matched with particular loads. It only approximates the location of the MPP because they are basically associated with specific insolation and load conditions [9].

Manuscript received December 2, 2000; revised May 28, 2002. This work was supported by a Grant from CityU under Projects 7001211 and 7100152, and a Central Allocation Grant from the Hong Kong Government under Project City U 1/00C. Recommended by Associate Editor K. Smedley.

K. K. Tse is with the Johnson Electric Group, N.T. Hong Kong.

M. T. Ho, H. S. H. Chung, and S. Y. R. Hui are with the Department of Electronic Engineering, City University of Hong Kong, Kowloon, Hong Kong (e-mail: eeshc@cityu.edu.hk).

Digital Object Identifier 10.1109/TPEL.2002.805594

The curve-fitting technique requires prior examination of the solar panel characteristics, so that an explicit mathematical function for describing the output characteristics is formulated. Although this technique attempts to track the MPP without computing the voltage–current product explicitly for the panel power, the curve-fitting technique cannot predict the characteristics including other complex factors, such as aging, temperature, and a possible breakdown of individual cells [4].

The perturb-and-observe (PAO) method is an iterative approach that perturbs the operation point of the PV system, in order to find the direction of change for maximizing the power. It is operated by periodically perturbing the panel terminal voltage and comparing the PV output power with that of the previous perturbation cycle. Maximum power control is achieved by forcing the derivative of the power to be equal to zero under power feedback control. This has an advantage of not requiring the solar panel characteristics. However, this approach is unsuitable for applications in rapidly changing atmospheric conditions [9]. The PV panel power is measured by multiplying its voltage and current, using either a microprocessor or an analog multiplier. In [7], the tracking technique is based on the fact that the terminal voltage of panels at MPP is approximately at 76% of the open-circuit voltage. Thus, the controlled panel is disconnected from the load momentarily so that the open-circuit voltage can be sampled and kept as reference for the control loop. Recently, a simple MPPT tracker (MPPT) with similar approach, which is based on creating an inherent attractor at the MPP, has been proposed in [10]. It does not require external control and perturbation.

The disadvantage of the PAO method can be improved by comparing the instantaneous panel conductance with the incremental panel conductance. This incremental conductance technique (ICT) is the most accurate one among the other methods. The input impedance of a switching converter is adjusted to a value that can match the optimum impedance of the connected PV panel. This technique gives a good performance under rapidly changing conditions. However, the implementation is usually associated with a microcomputer or digital signal processor that usually increases the whole system cost.

Concluding the above discussions, one of the most desirable approaches of implementing a MPP tracker is to use the ICT without requiring sophisticated digital sampling or mathematical manipulations. Moreover, the realization should be of low-cost and high accuracy and control capability. In this paper, a novel technique for efficiently maximizing the output power of a solar panel supplying to a load or battery bus under

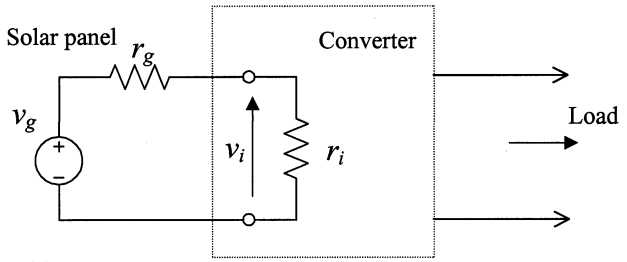

Fig. 1. Thevenin's equivalent circuit of a solar panel connecting to a converter.

varying meteorological conditions is presented. The power conversion stage (PCS), which is connected between a solar panel and a load or battery bus, is a pulsewidth-modulated (PWM) dc/dc SEPIC or Cuk converter or their derived circuits operating in discontinuous inductor current mode (DICM) or capacitor voltage mode (DCVM). These two types of converters were found to have the input resistance characteristics being proportional or inversely proportional to the switching frequency. Hence, by adjusting the nominal duty cycle of the main switch in the converter, the input resistance of the converter can be made equal to the equivalent output resistance of the panel. This operation ensures the maximum power transfer. By modulating a small-signal sinusoidal perturbation into the switching frequency of the main switch and comparing the ac component and average value of the panel terminal voltage, the MPP can be located. The tracking capability of the proposed technique has been verified experimentally with a 10 W solar cell panel at different insolation (incident solar radiation) levels and temperatures, and under different large-signal insolation changes.

II. Operating Principles

Fig. 1 shows an equivalent circuit of the solar array connecting to a MPP tracker. The solar array is modeled by a Thevenin's equivalent circuit, which consists of a voltage source v_g connected in series with an output resistance r_g around the MPP. Both v_g and r_g are subject to the level of insolation and temperature. The input voltage and equivalent input resistance of the converter are v_i and r_i, respectively. Assuming no converter loss, the input power P_i going into the tracker is equal to the output power P_o of the solar array

$$P_i = P_o = \frac{v_i^2}{r_i}. \tag{1}$$

The rate change of P_i with respect to v_i and r_i can be shown to be

$$\partial P_i = 2\,\frac{v_i}{r_i}\,\partial v_i - \frac{v_i^2}{r_i^2}\,\partial r_i. \tag{2}$$

At the MPP, the rate of change of P_i equals zero and r_i equals r_g. Hence

$$\frac{\delta v_i}{\delta r_i} \approx \frac{\partial v_i}{\partial r_i} = \frac{V_i}{2r_g} \tag{3}$$

where V_i is the average input voltage. This equation gives the required dynamic input characteristics of the tracker at the MPP

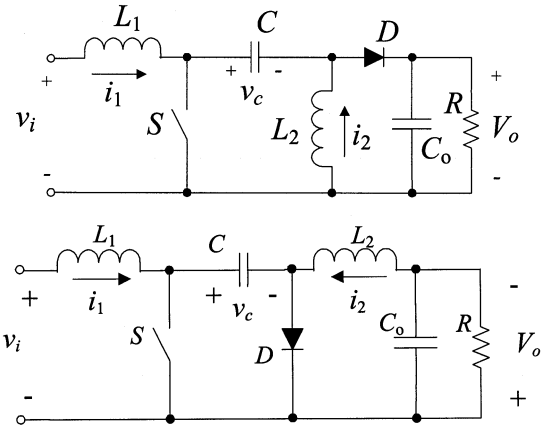

Fig. 2. Circuit diagram of the SEPIC and Cuk converter. (a) SEPIC. (b) Cuk converter.

where v_i has small-signal variation of δv_i subject to a small-signal change of δr_i.

In Fig. 1, the converter that connects to the solar panel is a SEPIC or Cuk converter operating in DICM or DCVM [11], [12]. The tracking operations are described as follows.

A. Discontinuous Inductor Current Mode (DICM)

Since the input characteristics of SEPIC and Cuk converters (Fig. 2) are similar, the input resistance r_i equals

$$r_i = \frac{2L_e f_S}{d^2} \tag{4}$$

where $L_e = L_1 // L_2$, f_S is the switching frequency, and d is the duty cycle of the switch S in Fig. 2. Detailed proof of (4) is shown in the Appendix.

By differentiating (4) with respect to f_S, it can be seen that a small change of f_S will introduce a small variation in r_i. That is

$$\delta r_i = \frac{2L_e}{d^2}\,\delta f_S. \tag{5}$$

Hence, injecting a small-signal sinusoidal variation into f_S gives

$$f_S = \overline{f}_S + \delta f_S = \overline{f}_S + \hat{f}_S \sin(2\pi f_m t) \tag{6}$$

where $\overline{f}_S$ is the nominal switching frequency, f_m is the modulating frequency and is much lower than $\overline{f}_S$, and $\hat{f}_S$ is the maximum frequency deviation.

Thus, with the above switching frequency perturbation, r_i will include an average resistance R_i and a small variation δr_i. That is,

$$r_i = R_i + \delta r_i, \tag{7}$$

where

$$R_i = \frac{2L_e}{d^2}\,\overline{f}_S, \tag{8}$$

and

$$\delta r_i = \frac{2L_e}{d^2}\,\hat{f}_S \sin(2\pi f_m t). \tag{9}$$

Let D_{MP} be the required duty cycle of the switch S at MPP. r_g can be expressed as

$$r_g = \frac{2L_e\overline{f}_S}{D_{MP}^2}. \tag{10}$$

By using (8) and (10)

$$V_i = \frac{R_i}{R_i + r_g}\, v_g = \frac{D_{MP}^2}{D_{MP}^2 + d^2}\, v_g \tag{11}$$

and the variation of v_i with respect to r_i becomes

$$\delta v_i \approx \frac{d}{dr_i}\left(\frac{r_i}{r_i + r_g}\, v_g\right)\delta r_i = \frac{r_g v_g}{(R_i + r_g)^2}\,\delta r_i. \tag{12}$$

By substituting (5), (8), and (10) into (12), the small-signal variation on v_i is

$$\delta v_i = \frac{(D_{MP}d)^2 v_g}{(D_{MP}^2 + d^2)^2\overline{f}_S}\,\delta f_S. \tag{13}$$

The peak value of δv_i (i.e., $\hat{v}_i$) becomes

$$\hat{v}_i = \frac{(D_{MP}d)^2 v_g}{(D_{MP}^2 + d^2)^2\overline{f}_S}\,\hat{f}_S. \tag{14}$$

As v_g and r_g vary with insolation and temperature, d should be automatically adjusted to D_{MP} in the controller. The following equation holds at the MPP and is obtained by substituting (5) and (8) into (3)

$$\frac{\hat{f}_S}{2\overline{f}_S}\, V_i = \hat{v}_i. \tag{15}$$

Based on (11) and (14), the difference, ε_1, between the normalized characteristics of $\hat{f}_S V_i/2\overline{f}_S v_g$ and $\hat{v}_i/v_g$ can be shown to be equal to

$$\begin{aligned}\varepsilon_1(k) &= \frac{\hat{f}_S V_i}{2\overline{f}_S v_g} - \frac{\hat{v}_i}{v_g} \\ &= \beta\frac{V_i}{v_g} - \frac{\hat{v}_i}{v_g} \\ &= \beta\left[\frac{D_{MP}^2}{D_{MP}^2 + d^2}\right] - 2\beta\left[\frac{(D_{MP}d)^2}{(D_{MP}^2 + d^2)^2}\right] \\ &= \beta\left[\frac{1}{1+k^2}\right] - 2\beta\left[\frac{k^2}{(1+k^2)^2}\right] \\ &= \beta\frac{1-k^2}{(1+k^2)^2}\end{aligned} \tag{16}$$

where $k = d/D_{MP}$ and $\beta = \hat{f}_S/(2\overline{f}_S)$.

Fig. 3 shows the relationships between ε_1/β and k. It can be concluded that

$$\text{If } d < D_{MP}\,(\text{i.e., } k<1),\ \varepsilon_1(k) > 0 \tag{17a}$$
$$\text{If } d = D_{MP}\,(\text{i.e., } k=1),\ \varepsilon_1(1) = 0 \tag{17b}$$
$$\text{If } d > D_{MP}\,(\text{i.e., } k>1),\ \varepsilon_1(k) < 0. \tag{17c}$$

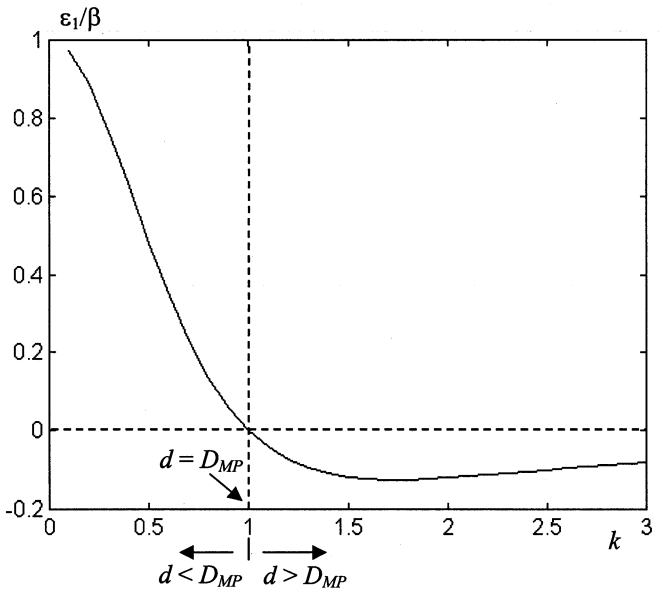

Fig. 3. Relationships between ε_1/β and k.

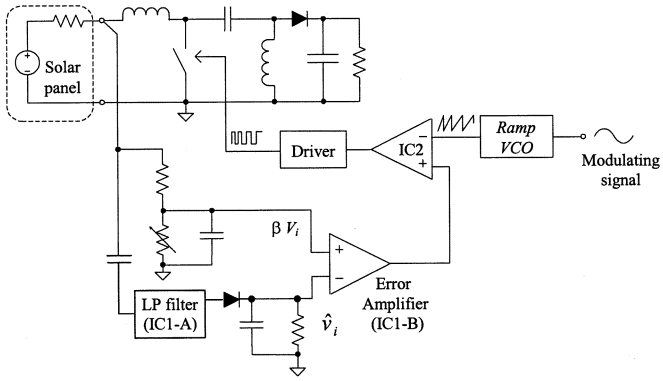

Fig. 4. Proposed MPP tracking method.

Based on (17), the proposed MPP tracking method is depicted in Fig. 4. f_S is modulated with a small-signal sinusoidal variation. V_i and $\hat{v}_i$ are sensed. V_i is then scaled down by the factor of β and is compared with $\hat{v}_i$. $\hat{v}_i$ is obtained by using a peak detector to extract the value of the ac component in v_i. The switching frequency component in v_i is removed by using a low-pass (LP) filter. The error amplifier controls the PWM modulator to locate d at D_{MP}. If $\hat{v}_i$ is smaller than $(\hat{f}_s/2\overline{f}_s)V_i$, $\varepsilon_1 > 0$. The output of the error amplifier, and hence d, will be increased. Conversely, d will be decreased until $d = D_{MP}$. The cutoff frequency of the error amplifier is set to be much lower than the modulating frequency f_m. It can be seen from the above that the proposed technique will keep track the output characteristics of solar panels without approximating the voltage–current relationships.

B. Discontinuous Capacitor Voltage Mode (DCVM)

In this mode, r_i equals

$$r_i = \frac{(1-d)^2}{2f_S C}. \tag{18}$$

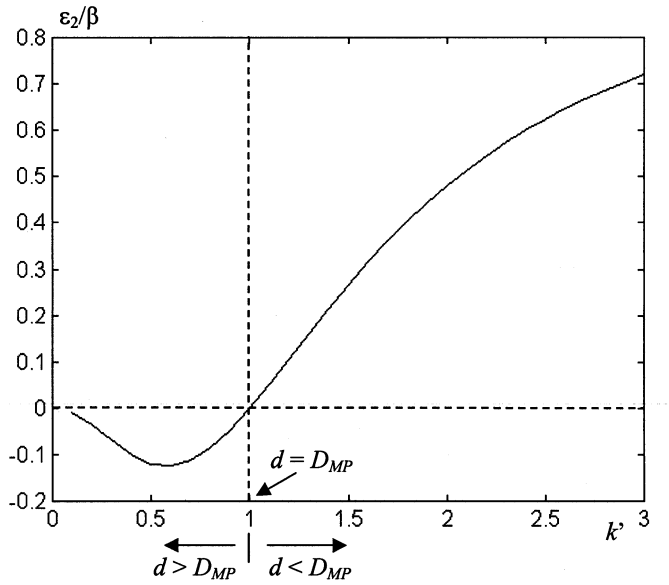

Fig. 5. Relationships between ε_2/β and k'.

Thus, δr_i with respect to the frequency variation δf_S is

$$\delta r_i = -\frac{(1-d)^2}{2\overline{f}_S^2 C}\,\delta f_S. \tag{19}$$

Similar to deriving (11) and (13), it can be shown that

$$V_i = \frac{(1-d)^2}{(1-d)^2+(1-D_{MP})^2}\,v_g \tag{20}$$

and

$$\hat{v}_i = \frac{(1-d)^2(1-D_{MP})^2 v_g}{[(1-d)^2+(1-D_{MP})^2]^2\overline{f}_S}\,\hat{f}_S. \tag{21}$$

By substituting $d = D_{MP}$ into (20) and (21), (15) is still valid. Again, the difference, ε_2, between the nominal characteristics of $\hat{f}_S V_i/2\overline{f}_S v_g$ and $\hat{v}_i/v_g$ can be shown to be

$$\begin{aligned}\varepsilon_2(k') &= \frac{\hat{f}_S V_i}{2\overline{f}_S v_g} - \frac{\hat{v}_i}{v_g}\\ &= \beta\frac{V_i}{v_g} - \frac{\hat{v}_i}{v_g}\\ &= \beta\left[\frac{(1-d)^2}{(1-d)^2+(1-D_{MP})^2}\right]\\ &\quad - 2\beta\left[\frac{(1-d)^2(1-D_{MP})^2}{[(1-d)^2+(1-D_{MP})^2]^2}\right]\\ &= \beta\left[\frac{k'^2}{k'^2+1}\right] - 2\beta\left[\frac{k'^2}{(k'^2+1)^2}\right]\\ &= \beta\,\frac{k'^2(k'^2-1)}{(k'^2+1)^2}\end{aligned} \tag{22}$$

where $k' = (1-d)/(1-D_{MP})$.

TABLE I
COMPARISONS OF THE CONVERTER BEHAVIORS IN DICM AND DCVM

	DICM	DCVM
M	$\frac{d}{d_1}$	$\frac{d_1}{1-d}$
r_i	$\frac{2L_e f_S}{d^2}$	$\frac{(1-d)^2}{2 f_S C}$
ΔI_1	$\frac{2L_2}{d(L_1+L_2)} I_1$	Negligible as $L_1 >> \frac{1}{(2\pi f_S)^2 C}$
$V_{s,max}$ and $V_{D,max}$	$(1+M)V_i$	$\frac{2M}{d_1} V_i$
$I_{s,max}$ and $I_{D,max}$	$\frac{2}{M d_1} I_1$	$(1+\frac{1}{M}) I_1$
d_1	$\sqrt{2L_e f_S / R}$	$\sqrt{2R f_S C}$
Condition of d	$< 1-d_1$	$> d_1$
Application	High voltage, low current	Low voltage, high current
Recommended arrangement for solar panels	Series connection	Parallel connection

Fig. 5 shows the relationships between ε_2/β and k'. Similar behaviors as in (17) are obtained

$$\text{If } d < D_{MP}(k' > 1),\ \varepsilon_2(k') > 0 \tag{23a}$$
$$\text{If } d = D_{MP}(k' = 1),\ \varepsilon_2(1) = 0 \tag{23b}$$
$$\text{If } d > D_{MP}(k' < 1),\ \varepsilon_2(k') < 0. \tag{23c}$$

Hence, the control method used in DICM can also be applied to the DCVM.

C. Comparison of DICM and DCVM

Although a converter operating in DICM and DCVM can perform the MPP tracking, selection of a suitable operating mode is based on several extrinsic and intrinsic characteristics. Table I shows a comparison of the converter behaviors in DICM and DCVM. Detailed proofs of the entries in Table I are given in the Appendix.

For the extrinsic characteristics, apart from the difference in the voltage conversion ratio M, the input current ripple ΔI_1 in the DCVM is smaller than that in the DICM. Thus, variation of the panel-converter operating point in the DCVM is smaller. This can effectively operate the panel at the near MPP [13]. Nevertheless, input current perturbation is designed to be less than 10% in the implementation.

In order to ensure that the converter is operating in the DICM

$$d < 1 - \sqrt{\frac{2L_e f_s}{R}} = \frac{V_o}{V_o + V_i}. \tag{24}$$

Thus, (24) gives the maximum duty cycle of S for a given load resistance.

In order to ensure that the converter is operating in DCVM

$$d > \sqrt{2Rf_s C} = \frac{V_o}{V_o + V_i}. \tag{25}$$

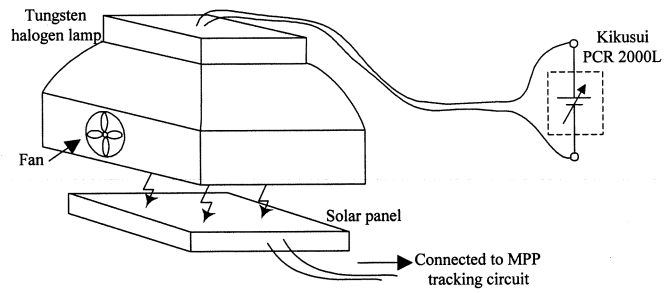

Fig. 6. Experimental setup for studying the proposed MPP tracking technique.

TABLE II
COMPONENT VALUES OF THE TWO CONVERTERS

	DICM	DCVM
L_1	2.2mH	2.2mH
L_2	25μH	450μH
C	100μF	47nF
C_o	1mF	1mF
R	10Ω	10Ω
$\bar{f}_s$	50kHz	50kHz
$\hat{f}_s$	5kHz	5kHz
f_m	1kHz	1kHz

Equation (25) gives the minimum duty cycle of S for a given load resistance.

For the intrinsic characteristics, the voltage stress $V_{S,\max}$ of S in the DCVM is higher than that in the DICM under the same panel terminal voltage and voltage conversion ratio. Conversely, the current stress $I_{S,\max}$ in the DICM is higher than that in the DCVM with the same panel output current. Thus, for the same panel power, DICM is more suitable for panel in series connection whilst DCVM is for parallel connection.

III. EXPERIMENTAL VERIFICATION

The experiment setup for studying the proposed MPP tracking technique is shown in Fig. 6. A solar panel Siemens SM-10 with a rated output power of 10 W is used. Two SEPIC's, which are operating in DICM and DCVM, respectively, have been prototyped. The component values of the two converters are tabulated in Table II. The switching frequency is 50 kHz. The modulating frequency f_m is 1 kHz. The maximum frequency deviation $\hat{f}_s$ is 5 kHz (10%). Based on Table I and (4), the maximum value of d is 0.5 for the converter in DICM. The minimum panel output resistance that can be matched by the converter is 9.8 Ω. For the converter in DCVM, based on Table I and (18), the minimum value of d is 0.217. The maximum panel output resistance that can be matched is 130.5 Ω. The

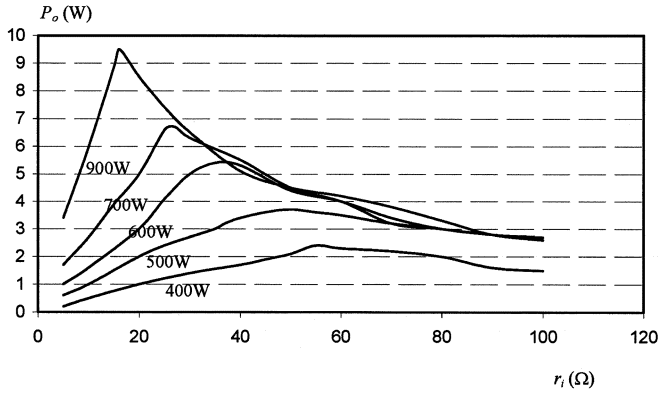

Fig. 7. $P_o - r_i$ characteristics of the solar panel at different P_{lamp}.

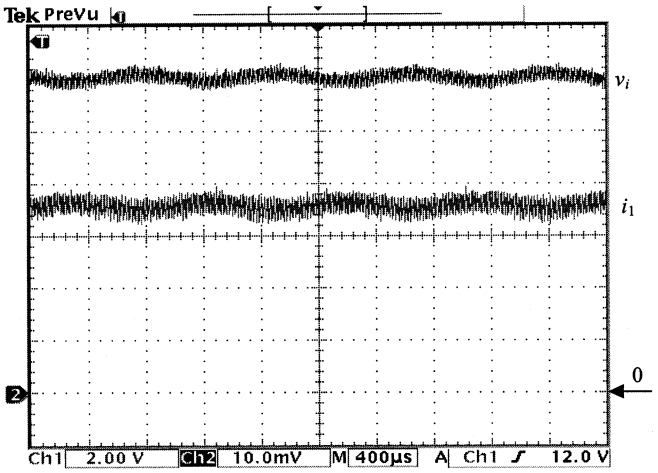

(a)

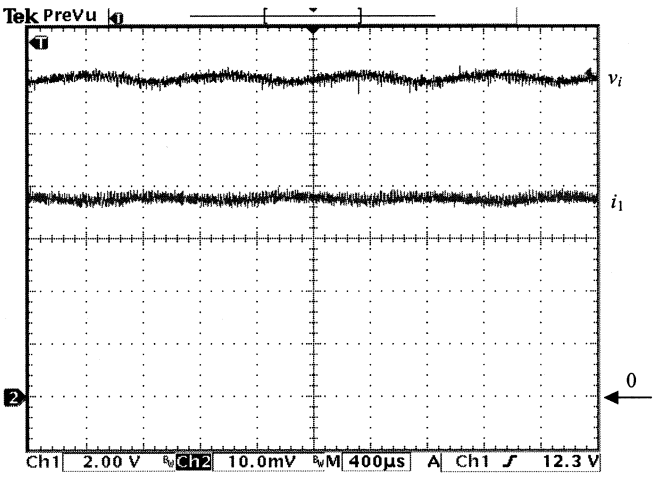

(b)

Fig. 8. Experimental waveforms of v_i and i_1 of the two SEPIC prototypes at the MPP when P_{lamp} equals 900 W. (a) DICM (v_i: 2 V/div. i_1: 0.2 A/div.). (b) DCVM (v_i: 2 V/div. i_1: 0.2 A/div.).

surface temperature of the panel is kept at about 40 °C throughout the test. The radiation illuminated is adjusted by controlling the power of a 900 W tungsten halogen lamp using a programmable dc supply source—Kikusui PCR 2000L. Fig. 7 shows the $P_o - r_i$ characteristics of the solar panel at

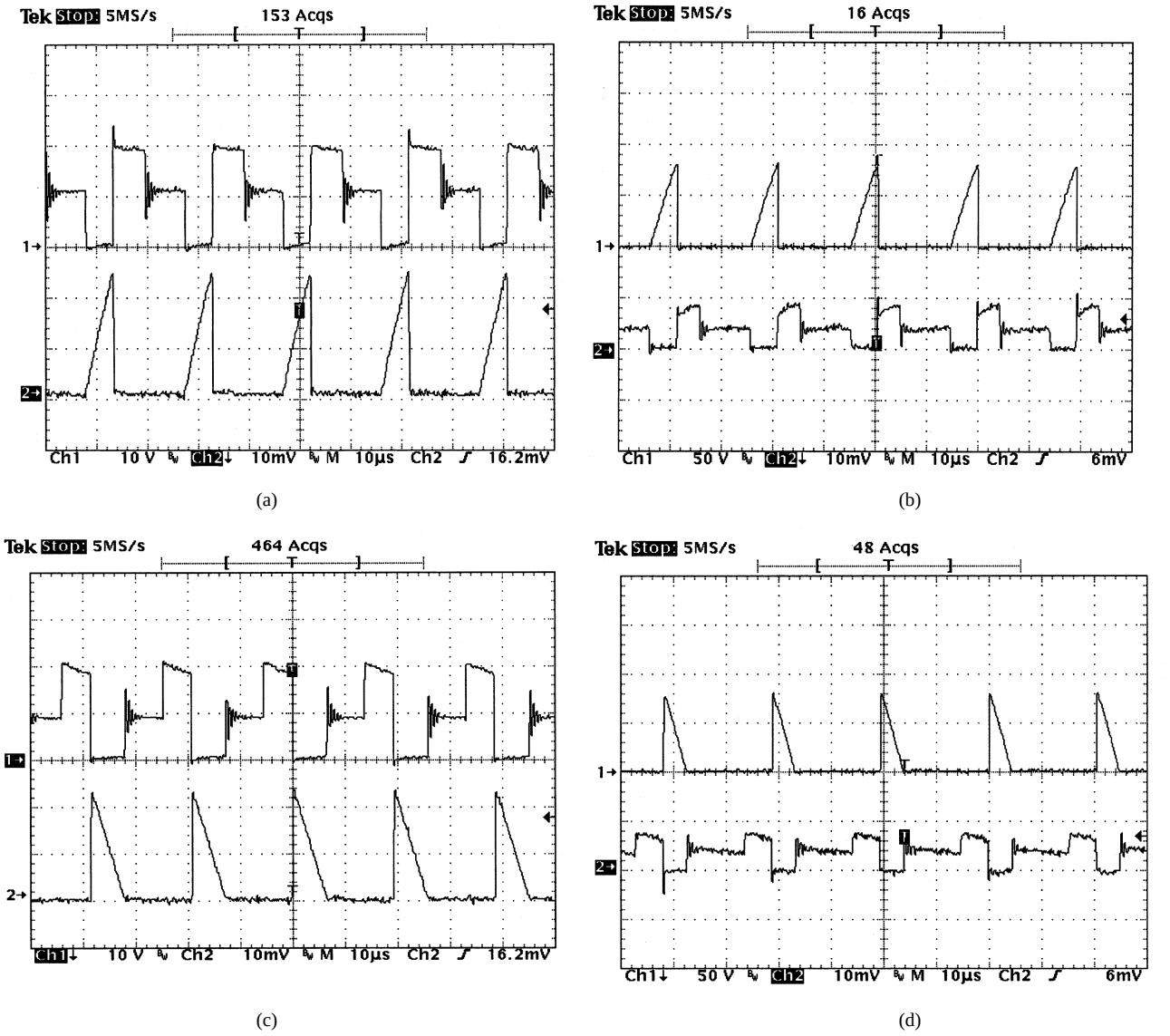

Fig. 9. Experimental voltage and current stresses on S and D. (Timebase: 10 μs/div). (a) Voltage and current stresses on S in DICM. (Ch1: 10 V/div. Ch2: 2 A/div.). (b) Voltage and current stresses on S in DCVM. (Ch1: 50 V/div. Ch2: 2 A/div.). (c) Voltage and current stresses on D in DICM. (Ch1: 10 V/div. Ch2: 2 A/div.). (d) Voltage and current stresses on D in DCVM. (Ch1: 50 V/div. Ch2: 2 A/div.).

different P_{lamp}. It can be seen that the output resistance of the panel at MPP varies from 18 Ω to 58 Ω when P_{lamp} is changed from 900 W to 400 W. The operating range is within the tracking capacity (i.e., the input resistance) of the two converters. Since upon a maximum of 10% of perturbation, r_i will also be deviated from the MPP by about 10%. However, referring to Fig. 7, the resultant average power drawn from the solar panel is still more than 90% of the maximum extractable power for all P_{lamp}. Fig. 8 shows the experimental waveforms of v_i and i_1 of the two prototypes at the MPP when P_{lamp} equals 900 W. It can be seen that v_i has a small sinusoidal perturbation of 1 kHz. Fig. 9 shows the experimental voltage and current stresses on S and D in the two converters. As expected, the current stresses on S and D in the DICM are about three times higher than that in the DCVM, whilst the voltage stresses on S and D in the DCVM are four times higher than that in the DICM. These confirm the theoretical prediction (see Table III).

TABLE III
TRACKING EFFICIENCY OF THE PROPOSED METHOD

P_{lamp} (W)	Maximum Extractable Power (W)	Power Extracted (W)		Tracking Efficiency (%)	
		DICM	DCVM	DICM	DCVM
400	2.4	2.3	2.2	95.8	91.7
500	3.7	3.5	3.6	94.6	97.3
600	5.4	5.2	5.0	96.3	92.6
700	6.7	6.5	6.6	97.0	98.5
800	8.0	7.8	7.9	97.5	98.8
900	9.5	9.4	9.2	98.9	96.8

An insolation change is simulated by suddenly changing P_{lamp} from 400 W to 900 W. The transient waveforms of v_i

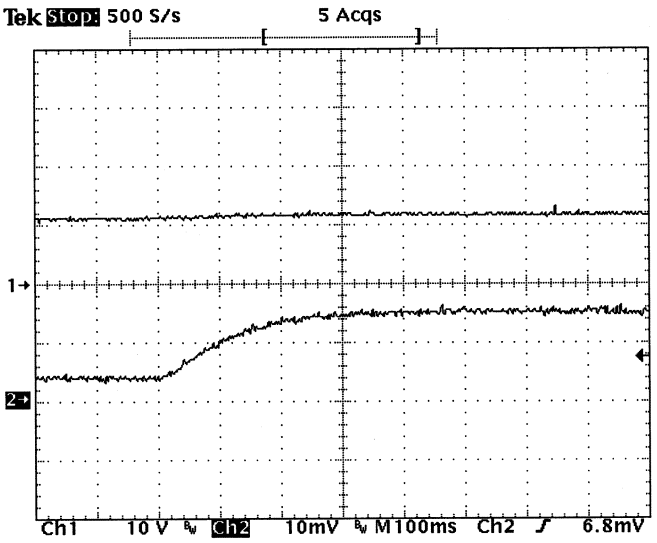

(a)

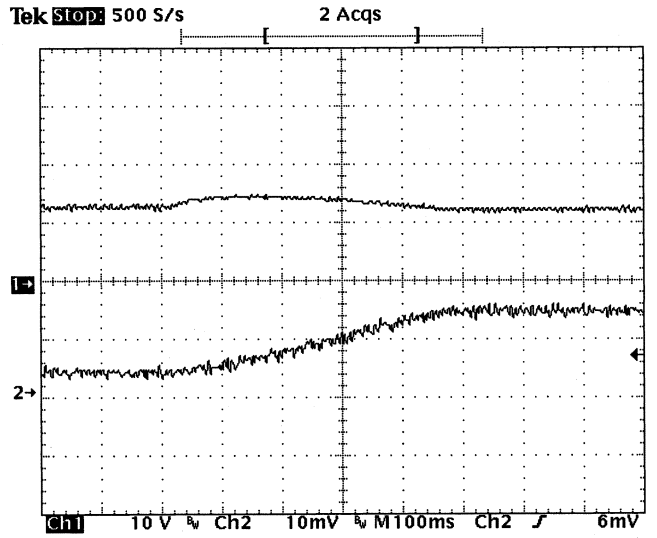

(b)

Fig. 10. Transient waveforms of the SEPIC converters when P_{lamp} is subject to a change from 400 W to 900 W. (Ch1: V_i, 10 V/div. Ch2: I_1, 0.5 A/div.) (a) DICM. (b) DCVM.

and i_i of the two converters are given in Fig. 10. It was found that both converters can perform the MPP tracking function and the panel output power is increased from 2.5 W to 9.5 W in 0.3 s in both cases. The tracked power is in close agreement with the measurements in Fig. 7.

IV. Conclusion

A novel technique for efficiently extracting the maximum output power from the solar panel is presented. A PWM dc/dc SEPIC or Cuk converter operating in discontinuous inductor–current or capacitor–voltage mode is used to match with the output resistance of the panel. By injecting the switching frequency with a small-signal sinusoidal variation and comparing the maximum variation and the average value at the input voltage, the MPP can be located. This method is simple and elegant without requiring any digital computation and approximation of the panel characteristics. Further research will be dedicated into a more in-depth study of the design of the error amplifier.

Appendix

Referring to Fig. 2 for SEPIC and Cuk converters, the average voltage across each inductor is zero whilst the average voltage across C, V_c, is as follows.

For SEPIC

$$V_c = V_i. \tag{A1}$$

For Cuk converter

$$V_c = V_i + V_o. \tag{A2}$$

The voltage conversion ratio, input resistance, input current ripple, maximum voltage and current stress on S and D in the DICM and DCVM are derived in the following sections.

A. Discontinuous Inductor Current Mode (DICM)

The capacitor voltages are constant throughout a switching period T_s. Under the steady state, the theoretical voltage and current waveforms are shown in Fig. 11(a). i_1 and i_2 are expressed as

$$i_1(t) = \begin{cases} \dfrac{v_i}{L_1}\,t + \alpha; & 0 < t < dT_s \\ -\dfrac{v_i}{L_1}\,t + \dfrac{(v_i + v_o)}{L_1} & \\ \quad dT_s + \alpha; & dT_s < t < (d+d_1)T_s \\ \alpha; & (d+d_1)T_s < t < T_s \end{cases} \tag{A3}$$

$$i_2(t) = \begin{cases} \dfrac{v_i}{L_2}\,t - \alpha; & 0 < t < dT_s \\ -\dfrac{v_o}{L_2}\,t + \dfrac{(v_i + v_o)}{L_2} & \\ \quad dT_s - \alpha; & dT_s < t < (d+d_1)T_s \\ -\alpha; & (d+d_1)T_s < t < T_s. \end{cases} \tag{A4}$$

Their average values I_1 and I_2 are equal to

$$I_1 = \frac{1}{T_s}\int_0^{T_S} i_1\,dt = \frac{V_i}{2L_1}\,(d+d_1)\,dT_s + \alpha, \tag{A5}$$

$$I_2 = \frac{1}{T_s}\int_0^{T_S} i_2\,dt = \frac{V_i}{2L_2}\,(d+d_1)\,dT_s - \alpha. \tag{A6}$$

It should be noted that I_2 is equal to the average output current of the converters.

Based on the volt-second balance on the inductors in Fig. 11(a), the voltage conversion ratio M can be expressed as

$$\begin{aligned} V_i\,dT_S &= V_o\,d_1T_S \\ \Rightarrow \quad M &= \frac{V_o}{V_i} = \frac{d}{d_1}. \end{aligned} \tag{A7}$$

By using the input and output power balance equation of $V_iI_1 = V_oI_2$ and (A5)–(A7), it can be shown that

$$I_1 = \frac{V_i\,d^2T_S}{2L_e} \tag{A8}$$

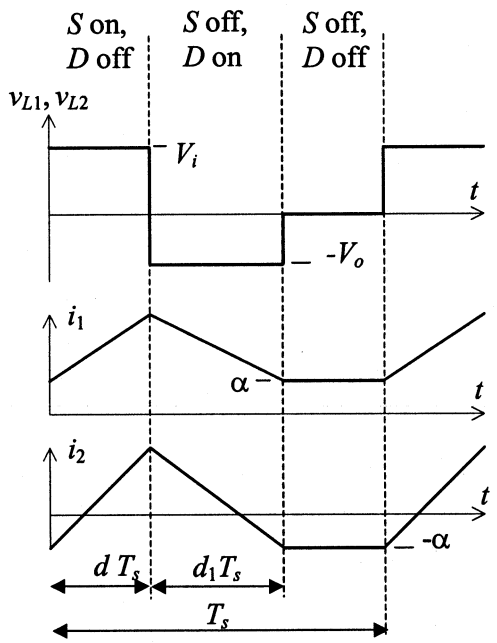

(a)

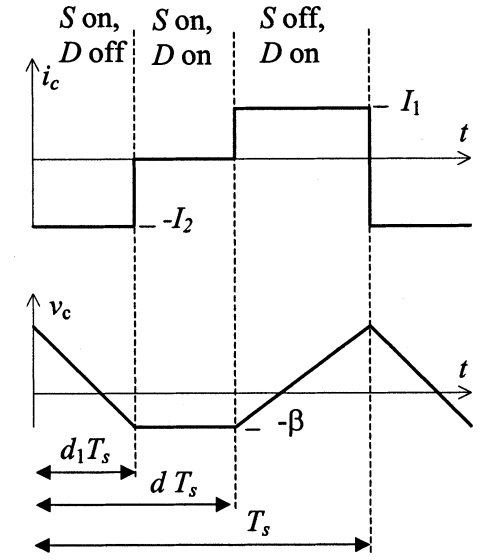

(b)

Fig. 11. Key waveforms of SEPIC and Cuk converter. (a) Voltage and current waveforms of L_1 and L_2 in DICM. (b) Current and voltage waveforms of C in DCVM.

where $L_e = L_1//L_2$. Hence, the input equivalent resistance is equal to

$$r_i = \frac{2L_e f_S}{d^2}. \tag{A9}$$

By using (A3), the input ripple ΔI_1 current is

$$\Delta I_1 = \frac{V_i}{L_1} dT_S. \tag{A10}$$

By substituting (A8) into (A10), it can be shown that

$$\Delta I_1 = \frac{2L_2}{d(L_1 + L_2)} I_1. \tag{A11}$$

In addition, d_1 can be obtained by considering the input and output power of

$$V_i I_1 = \frac{V_o^2}{R}. \tag{A12}$$

By substituting (A8) into (A12) and using (A7)

$$d_1 = \sqrt{2L_e f_S / R}. \tag{A13}$$

In order to ensure the operation in DICM, it can be observed from Fig. 11(a) that

$$d < 1 - d_1. \tag{A14}$$

Maximum voltage stress on S, $V_{S,\max}$, occurs in the time interval when S is off and D is on. Maximum voltage stress on D, $V_{D,\max}$, occurs when S is on and D is off. For SEPIC

$$V_{S,\max} = V_{D,\max} = V_o + V_c. \tag{A15}$$

For Cuk converter

$$V_{S,\max} = V_{D,\max} = V_c. \tag{A16}$$

After substituting (A1) into (A15) and (A2) into (A16), it can be observed that $V_{S,\max}$ and $V_{D,\max}$ are the same in the two converters, where

$$V_{S,\max} = V_{D,\max} = (1 + M)V_i. \tag{A17}$$

The maximum current stresses on S and D, $I_{S,\max}$ and $I_{D,\max}$, occurs at $t = dT_s$. It can be shown that

$$\begin{aligned} I_{S,\max} &= I_{D,\max} = i_1(dT_s) + i_2(dT_s) \\ &= \frac{2}{M\, d_1} I_1. \end{aligned} \tag{A18}$$

B. Discontinuous Capacitor Voltage Mode (DCVM)

As I_1 and I_2 are constant throughout T_S in this mode, the voltage waveforms of C, v_C, of the two converters are depicted in Fig. 11(b). It can be shown that

$$v_C(t) = \begin{cases} -\dfrac{I_2}{C} t + \dfrac{I_1(1-d)T_s}{C} - \beta & 0 < t < d_1 T_s \\ -\beta & d_1 T_s < t < dT_s \\ \dfrac{I_1}{C}(t - dT_s) - \beta & dT_s < t < T_s. \end{cases} \tag{A19}$$

Its average value V_C is equal to

$$\begin{aligned} V_C &= \frac{1}{T_S} \int_0^{T_S} v_C \, dt \\ &= \frac{T_S}{C} \left[I_1(1-d)(1-d+2d_1) - I_2 d_1^2 \right] - \beta, \end{aligned} \tag{A20}$$

where β equals V_o for SEPIC and zero for Cuk converter (see Fig. 11).

Based on the amp-second balance on C in Fig. 11(b) and input and output power balance, M can be expressed as

$$\begin{aligned} & I_1(1-d)T_S = I_2\, d_1 T_S \\ & \quad \Rightarrow \quad M = V_o/V_i = I_1/I_2 = d_1/(1-d). \end{aligned} \tag{A21}$$

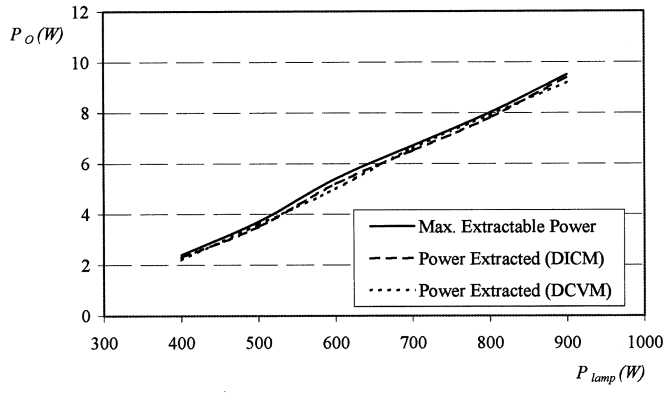

Fig. 12. Comparison of maximum solar panel output power using proposed method and the ideal ones in Fig. 7, under different P_{lamp}.

By substituting (A20) and (A21) into (A1) and (A2), it can be shown that

$$V_i = \frac{T_S}{2C} I_1 (1-d)^2. \tag{A22}$$

Hence, the input resistance r_i equals

$$r_i = \frac{(1-d)^2}{2Cf_S}. \tag{A23}$$

By substituting (A22) into (A12) and using (A21)

$$d_1 = \sqrt{2RCf_S}. \tag{A24}$$

In order to ensure the operation in DCVM, it can be observed from Fig. 11(b) that

$$d > d_1. \tag{A25}$$

Maximum voltage stresses on S and D occur at the time instant of T_S. For SEPIC

$$V_{S,\max} = V_{D,\max} = V_C(T_S) + V_o. \tag{A26}$$

For Cuk converter

$$V_{S,\max} = V_{D,\max} = V_c(T_S). \tag{A27}$$

By substituting (A19) and (A21) into (A26) and (A27), $V_{S,\max}$ and $V_{D,\max}$ are the same for the two converters and can be expressed as

$$V_{S,\max} = V_{D,\max} = \frac{2M}{d_1} V_1. \tag{A28}$$

Maximum current stress on S occurs at the time interval when S is on and D is off. Maximum current stress on D occurs at the time interval when S is off and D is on (Fig. 12). Thus

$$I_{S,\max} = I_{D,\max} = I_1 + I_2 = \left(1 + \frac{1}{M}\right) I_1. \tag{A29}$$

REFERENCES

[1] G. Foley, *Photovoltaic Applications in Rural Areas of the Developing World*. New York: World Bank Technical Paper, 1995.
[2] J. Applebaum, "The quality of load matching in a direct-coupling photovoltaic system," *IEEE Trans. Energy Conv.*, vol. 2, pp. 534–541, Dec. 1987.
[3] A. Braunstein and Z. Zinger, "On the dynamic optimal coupling of a solar cell array to a load and storage batteries," *IEEE Trans. Power Apparat. Syst.*, vol. 100, pp. 1183–1188, 1981.
[4] A. Kislovski and R. Redl, "Maximum-power-tracking using positive feedback," in *Proc. IEEE Power Electron. Spec. Conf.*, 1994, pp. 1065–1068.
[5] S. Wolf and J. Enslin, "Economical, PV maximum power point tracking regulator with simplistic controller," in *Proc. IEEE Power Electron. Spec. Conf.*, 1993, pp. 581–587.
[6] J. Gow and C. Manning, "Controller arrangement for boost converter systems sourced from solar photovoltaic arrays or other maximum power sources," *Proc. Inst. Elect. Eng.*, vol. 147, no. 1, pp. 15–20, Jan. 2000.
[7] J. Enslin, M. Wolf, D. Snyman, and W. Swiegers, "Integrated photovoltaic maximum power point tracking converter," *IEEE Trans. Ind. Electron.*, vol. 44, pp. 769–773, Dec. 1997.
[8] A. Nafeh, F. Fahmy, O. Mahgoub, and E. Abou El-Zahab, "Microprocessor control system for maximum power operation of PV arrays," *Int. J. Numer. Model.*, vol. 12, pp. 187–195, 1999.
[9] K. Hussein, I. Muta, T. Hoshino, and M. Osakada, "Maximum photovoltaic power tracking: An algorithm for rapidly changing atmosphere conditions," *Proc. Inst. Elect. Eng. G*, vol. 142, pp. 59–64, Jan. 1995.
[10] Y. Lim and D. Hamill, "Simple maximum power point tracker for photovoltaic arrays," *IEE Electron. Lett.*, vol. 36, no. 11, pp. 997–999, May 2000.
[11] B. Lin and Y. Lee, "Power-factor correction using Cuk converters in discontinuous-capacitor–voltage mode operation," *IEEE Trans. Ind. Electron.*, vol. 44, pp. 648–653, Oct. 1997.
[12] D. Maksimovic and S. Cuk, "A unified analysis of PWM converters in discontinuous modes," *IEEE Trans. Power Electron.*, vol. 6, pp. 476–490, Mar. 1991.
[13] R. Schmidt, F. Jenni, and J. Riatsch, "Control of an optimized converter for modular solar power generation," in *Proc. IEEE Int. Conf. Ind. Electron. Control Inst.*, 1994, pp. 479–484.

K. K. Tse (M'95) received the B.Eng. (with honors) degree in electrical engineering from The Hong Kong Polytechnic University, in 1995, and the Ph.D. degree from City University of Hong Kong, in 2000.

He was a Lecturer with the Institute of Vocational Education, Tsing Yi, (formerly Technical College), Hong Kong, in 1998. From 1999 to 2001, He was a Research Fellow with the Electronic Engineering Department, City University of Hong Kong. Since June 2001, he has been with Johnson Electric, Hong Kong, where he is currently a Technical Specialist in the R&D Department. He has published over 20 technical papers in the areas of his research interests, which include new numerical model methods and computer-aided simulation techniques, EMI reduction using random switching schemes for dc–dc converters, and new maximum power tracking technique for PV cells.

Dr. Tse received the First Prize in 1998 from the IEEE Postgraduate Student Paper Contest, Hong Kong Section, Third Prize in 1999 Region 10 IEEE Postgraduate Student Paper Contest, The Croucher Foundation Fellowship in 2000, and the Silver Award from the Young Inventor Competition, in December 2000.

M. T. Ho (S'02) was born in Hong Kong in 1979. He received the B.Eng. (with first class honors) degree in electronic engineering from the City University of Hong Kong in 2001 where he is currently pursuing the Ph.D. degree in power electronics.

His research interests include computer-aided simulation technique, photovoltaic panels power conversion, control methodologies, and inverter applications.

Mr. Ho received the Simatelex Charitable Foundation Scholarship.

Henry Shu-hung Chung (S'92–M'95) received the B.Eng. (with first class honors) degree in electrical engineering and the Ph.D. degree from The Hong Kong Polytechnic University, in 1991 and 1994, respectively.

Since 1995, he has been with the City University of Hong Kong. He is currently an Associate Professor in the Department of Electronic Engineering. His research interests include time-domain and frequency-domain analysis of power electronic circuits, switched-capacitor-based converters, random-switching techniques, digital audio amplifiers, soft-switching converters, and electronic ballast design. He has authored four research book chapters, and over 140 technical papers including 65 refereed journal papers in the current research area, and holds two U.S. patents.

Dr. Chung received the Grand Applied Research Excellence Award in 2001 from the City University of Hong Kong. He is currently IEEE student branch counselor and was Track Chair of the Technical Committee on Power Electronics Circuits and Power Systems, IEEE Circuits and Systems Society, from 1997 to 1998. He is presently an Associate Editor of the IEEE TRANSACTIONS ON CIRCUITS AND SYSTEMS—PART I: FUNDAMENTAL THEORY AND APPLICATIONS.

S. Y. (Ron) Hui (SM'94) was born in Hong Kong in 1961. He received the B.Sc. degree (with honors) from the University of Birmingham, U.K., in 1984, and the D.I.C. and Ph.D. degrees from the Imperial College of Science and Technology, University of London, London, U.K., in 1987.

He was a Lecturer in power electronics at the University of Nottingham, U.K., from 1987 to 1990. In 1990, he took up a lectureship at the University of Technology, Sydney, Australia, where he became a Senior Lecturer in 1991. He joined the University of Sydney in 1993 and was promoted to Reader of Electrical Engineering and Director of Power Electronics and Drives Research Group in 1996. Presently, he is a Chair Professor of Electronic Engineering and an Associate Dean of the Faculty of Science and Engineering at the City University of Hong Kong. He has published over 150 technical papers, including over 80 refereed journal publications. His research interests include all aspects of power electronics.

Dr. Hui received the Teaching Excellence Award in 1999 and the Grand Applied Research Excellence Award in 2001 from the City University of Hong Kong. He has been appointed an Honorary Professor by the University of Sydney, Australia since 2000.